Advances in Applied Mathematics and Mechanics
Adv. Appl. Math. Mech., Vol. **17**, No. 1, pp. 148-174

DOI: 10.4208/aamm.OA-2022-0243
February 2025

A Nonconvex and Nonsmooth Model for Deblurring Images under Cauchy Noise

Hongtao Chen and Weina Wang*

Department of Mathematics, Hangzhou Dianzi University, Hangzhou, Zhejiang 310018, China

Received 17 September 2022; Accepted (in revised version) 23 April 2023

Abstract. In this paper, we propose a nonconvex and nonsmooth model for image restoration with Cauchy noise removal. The regularization term is composed of a nonconvex Lipschitz potential function with first-order derivatives of an image, while the data fidelity term is introduced based on the maximum a posteriori estimator to Cauchy distribution. To handle the nonconvexity of regularizers, we adopt the proximal linearization technique to convert the original nonconvex model to a series of convex models, which can be easily implemented by alternating direction method with multipliers. Based on the Kurdyka-Łojasiewicz property, we can verify the global convergence of the proposed algorithm by using an abstract convergence framework. Numerical experiments and comparisons indicate that our method obtains good restorations and is effective for better preserving edges.

AMS subject classifications: 49K30, 49N45, 49N60, 90C26, 94A08, 94A12

Key words: Nonconvex and nonsmooth, Kurdyka-Łojasiewicz property, Cauchy noise, image restoration.

1 Introduction

In image processing, images are unavoidable to be degraded by blur and noise because of the limitation of imaging devices. Except for the common Gaussian noise [11, 29, 35, 37], Cauchy noise is another important type of additive noise appeared in wireless communication systems, biomedical images and synthetic aperture radar images [21,30,42]. In this paper, we focus on designing a nonconvex nonsmooth restoration model with globally convergent algorithm for deblurring images under Cauchy noise.

Without loss of generality, we rearrange an $n\times n$ image U into a vector $u\in\mathbb{R}^m$. Assume that $f\in\mathbb{R}^m$ is an observed image degraded from the true image $u\in\mathbb{R}^m$ with blur and

*Corresponding author.
Email: wnwang@hdu.edu.cn (W. Wang)

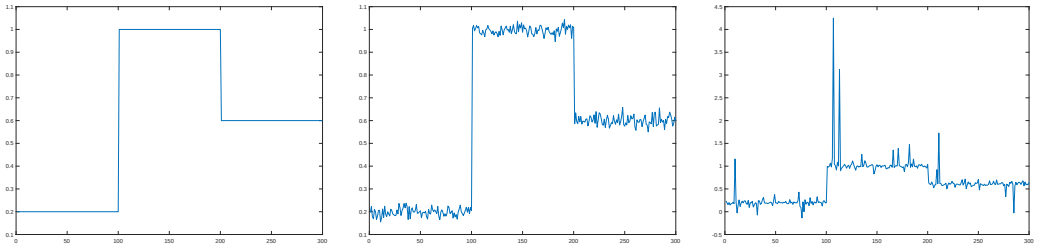

(a) Noise free signal (b) Signal with Gaussian noise (c) Signal with Cauchy noise

Figure 1: A 1D signal degraded by the Gaussian noise with mean 0 and variance 0.02 and the Cauchy noise with $\xi=0.02$.

Cauchy noise. Usually, the probability density function (PDF) of the Cauchy distribution is written as

$$p(x)=\frac{1}{\pi}\frac{\xi}{\xi^2+(x-\delta)^2},$$

where $\xi>0$ and $\delta\in\mathbb{R}$ are called the scale and localization parameters. The scale parameter determines the spread of the distribution around δ, while the localization parameter corresponds to the median of the distribution as discussed in [30]. In this paper, we consider $\delta=0$. From [30, 31], the Cauchy noise can be obtained from the ratio of two independent on Gaussian variables, and thus images corrupted by blur and Cauchy noise can be modeled as

$$f=Hu+\xi\frac{\eta_1}{\eta_2},$$

where $H=[h_1,h_2,\cdots,h_m]$ is a linear blur matrix, $\xi>0$ denotes the noise level, η_1 and η_2 are independent random variables following Gaussian distribution with mean 0 and variation 1. Some recent papers [21, 30, 31, 42] indicate that the Cauchy distribution has the heavy tails characteristic, which leads to noisy images having a greater probability to include outliers than that degraded by the Gaussian distribution. In Fig. 1, we show a simple example where a 1D signal is respectively corrupted by Gaussian noise and Cauchy noise. It is clear that the noisy signal degraded by Cauchy noise is impulsive. Interested readers can refer to more details about the differences between Gaussian, impulsive and Cauchy noise in [21,30,31,42].

A widely studied restoration method is based on variational regularization technique. One of the most popular variational models is ROF model [29] for Gaussian noise removal, where the total variation (TV) regularization term is the ℓ_1 norm of image gradient. Based on TV regularization, Sciacchitano et al. [30] introduced a variational model for recovering images degraded by Cauchy noise and blur as

$$\inf_{u\in BV(\Omega)}\int_\Omega |Du|+\frac{\alpha}{2}\int_\Omega \log(\gamma^2+(Hu-f)^2), \tag{1.1}$$

where $BV(\Omega)$ is the space of functions of bounded variation, $\int_\Omega |Du|$ is the TV term, $\int_\Omega \log(\gamma^2+(Hu-f)^2)$ is the data fidelity term and α is a positive model parameter. To get a strictly convex model, the authors in [30] added a quadratic penalty term to the nonconvex data fidelity term

$$\inf_{u\in BV(\Omega)} \int_\Omega |Du| + \frac{\alpha}{2}\left(\int_\Omega \log(\gamma^2+(Hu-f)^2)+\mu\|Hu-u_0\|^2\right), \tag{1.2}$$

where u_0 is the result restored by the median filter and $8\mu\gamma^2 \geq 1$. Since (1.2) is convex, it can be solved by many efficient algorithms which are irrespective of the initial condition. Under this idea, [12, 42] adopted other convex regularization terms with the convex data fidelity term to recover blurred images with Cauchy noise. For example, [42] proposed an adaptive model combining TV and high-order TV regularizations to reduce staircase artifacts. By using the alternating direction method with multipliers (ADMM), [21] introduced a globally convergent algorithm to solve the nonconvex model (1.1). However, its solution strongly depends on initializations and the solving scheme [42]. Later, [1, 16, 17, 20] presented different variational models with the nonconvex data fidelity term in (1.1) for Cauchy noise removal, and also used the nonconvex ADMM to obtain restorations. Similarly, these algorithms are dependent on the initializations. Moreover, other techniques [7,19,31,39,41,45], such as nonlocal myriad filters [19] and nonlinear diffusion equation [31], have been proposed to restore images corrupted by Cauchy noise. However, the high-order and nonlocal models are somewhat complicated to implement and time-consuming.

Instead of convex regularization models for image restoration, some studies [5, 9, 13, 15,23–25,38,40,44] have shown that nonconvex and nonsmooth potential functions composed of image gradient can enhance the gradient sparsity and produce neat edges with better contrast preservation. A great challenge is to design efficient numerical algorithms because of the nonsmooth of nonconvex gradient regularization. A widely used idea is to adopt smoothing approximation strategies [5, 8, 9, 15, 32] to convert nonsmooth terms into smooth forms, where the smoothed model can be solved by some classic optimization methods. Iterative reweighted ℓ_1 or ℓ_2 [10, 18] is another type of smoothing techniques to yield smoothed problems. Recently, iterative support shrinking algorithms were introduced [13, 14, 33, 34, 43] for handling nonconvex and non-Lipschitz restoration models. They put constraints on the support set of the gradient of images to remove nonsmooth points of the objective function, and then used the proximal linearization to change the original nonconvex model into a series of constrained convex models. As far as we know, most of nonconvex models with algorithms were designed to eliminate Gaussian noise [9, 13, 26, 34, 43]. It is necessary to explore new nonconvex nonsmooth methods to recover images from blurred images with Cauchy noise.

In this paper, we propose a nonconvex and nonsmooth regularization model for image restoration with Cauchy noise removal. It consists of a nonconvex potential function with first-order gradients of an image as the regularization term and the second term of (1.2) as the data fidelity term. A proximal linearization technique in [13] is adopted

to handle nonconvex Lipschitz regularizers, where the converted convex models can be easily solved by ADMM. Under an abstract convergence framework with the Kurdyka-Łojasiewicz property, the global convergence of the proposed algorithm is proved. Experimental results show that our method obtains good restorations and outperforms the TV based regularization model.

The paper is organized as follows. In Section 2, we present some basic notations, our model and the corresponding numerical algorithm. Section 3 gives the global convergence analyses. In Section 4, numerical experiments and comparisons are shown. At last, we conclude the paper in Section 5.

2 The proposed model and numerical algorithm

2.1 Basic notation

We first give the discrete difference operators of a grayscale image, which is represented as an $n\times n$ matrix. Denote $\mathbf{J}=\{(i_x,i_y):1\le i_x,i_y\le n\}$. For $U\in\mathbb{R}^{n\times n}$, the first-order difference operators at a pixel (i_x,i_y) are given as follows:

$$(D_x^+U)_{i_x,i_y}=\begin{cases} U_{i_x,i_y+1}-U_{i_x,i_y}, & 1\le i_y\le n-1,\\ U_{i_x,1}-U_{i_x,n}, & i_y=n,\end{cases}$$
$$(D_y^+U)_{i_x,i_y}=\begin{cases} U_{i_x+1,i_y}-U_{i_x,i_y}, & 1\le i_x\le n-1,\\ U_{1,i_y}-U_{n,i_y}, & i_x=n,\end{cases}$$

where D_x^+ and D_y^+ denote forward difference operators with periodic boundary condition.

When an image $U\in\mathbb{R}^{n\times n}$ is reformulated into a vector $u\in\mathbb{R}^m$ ($m=n^2$), the index set of all elements of u is denoted by $J=\{1,2,\cdots,m\}$. There is a one-to-one correspondence between J and $\mathbf{J}$, i.e., $J\to\mathbf{J}$: $i\mapsto(i_x,i_y)$, where

$$\begin{cases} i_x=\left\lfloor\dfrac{i}{n}\right\rfloor+1, & i_y=\mathrm{mod}(i,n), \quad \mathrm{mod}(i,n)\neq 0,\\ i_x=\dfrac{i}{n}, & i_y=n, \qquad\qquad \mathrm{mod}(i,n)=0.\end{cases}$$

Define the discrete gradient operator d_i as $d_i=\left(d_i^x,d_i^y\right)^T\in\mathbb{R}^{2\times m}$, where $d_i^x,d_i^y\in\mathbb{R}^{1\times m}$ and $d_i^xu=(D_x^+U)_{i_x,i_y}$, $d_i^yu=(D_y^+U)_{i_x,i_y}$. Let $D=\left(d_1,d_2,\cdots,d_m\right)^T\in\mathbb{R}^{2m\times m}$ be the first-order matrix. The Euclidean norm is denoted as $\|\cdot\|$.

Moreover, the definitions of $\widehat{\partial}$, ∂ are given as follows.

Definition 2.1 (Subdifferentials [28]). *Let $h:\mathbb{R}^m\to(-\infty,+\infty]$ be a proper and lower semicontinuous function. For a point $x\in\mathrm{dom}\,h$,*

1. *the regular subdifferential of h at x is defined as*

$$\widehat{\partial}h(x)=\left\{w\in\mathbb{R}^n:\liminf_{z\neq x\, z\to x}\frac{h(z)-h(x)-\langle w,z-x\rangle}{\|z-x\|}\geq 0\right\},$$

where z is a point near x but different from x.

2. *the limiting subdifferential of h at x is defined as*

$$\partial h(x)=\{w\in\mathbb{R}^n:\exists x^k\to x, h(x^k)\to h(x)\ \ and\ \ w^k\in\widehat{\partial}h(x^k)\to w\ \ as\ \ k\to\infty\}.$$

Remark 2.1. (a) For each $x\in\operatorname{dom}h$, we have $\widehat{\partial}h(x)\subseteq\partial h(x)$. If h is differentiable at x, then

$$\widehat{\partial}h(x)=\partial h(x)=\{\nabla h(x)\}.$$

(b) A point $x\in\mathbb{R}^m$ is called a critical point if $0\in\partial h(x)$.

2.2 Nonconvex model

To remove blur and Cauchy noise, we propose the following nonconvex and nonsmooth model

$$(\mathcal{P})\quad \min_{u\in\mathbb{R}^m}F(u):=\sum_{i\in J}\varphi(\|d_iu\|)+\frac{\alpha}{2}\left(\langle\log(\gamma^2+(Hu-f)^2),\mathbf{1}\rangle+\mu\|Hu-u_0\|^2\right),\qquad(2.1)$$

where $\|d_iu\|=\sqrt{(d_i^xu)^2+(d_i^yu)^2}$, $\varphi(t)$ is a nonconvex potential function, the logarithmic function log is pixel-by-pixel, u_0 is the pre-denoising result of the median filter, $\mathbf{1}=(1,1,\cdots,1)^T\in\mathbb{R}^m$, μ is a positive penalty parameter and α is a positive model parameter. In the proposed model, the first nonconvex and nonsmooth term composed of first-order derivatives can preserve important structures of u, while the second term with a quadratic penalty is the data fitting term to ensure the convexity under $8\mu\gamma^2\geq 1$.

For the potential function $\varphi(t)$ and the proposed model (2.1), some basic assumptions are listed below.

Assumption 2.1. (a) $\varphi(t):[0,+\infty)\to[0,+\infty)$ is concave and coercive, and $\varphi(0)=0$.

(b) $\varphi(t)$ is C^1on $[0,+\infty)$, $\varphi'(t)|_{[0,+\infty)}>0$ and $\varphi(t)$ is L-Lipschitz gradient continuous.

(c) The minimizer of $(\mathcal{P})$ always exists.

In the image processing, the nonconvex Lipschitz potential function $\varphi(t)$ satisfying Assumption 2.1 may be $\ln(1+at)$ $(a>0)$ and $(t+\epsilon)^p$ $(0<p<1$ and $\epsilon>0)$ as that in [9,13,25].

Algorithm 2.1 IIAPL: Inexact iterative algorithm with a proximal linearization for (2.1).

1. Input $\alpha, H, f, \rho > 0$. Initialize $u^0 = f$.
2. For each $k = 0,1,\cdots$, compute u^{k+1} as an approximation solution of

$$\min_{u\in\mathbb{R}^m} \; H_k(u) := \sum_{i\in J} \varphi'(\|d_i u^k\|)\|d_i u\| + \frac{\rho}{2}\|u-u^k\|^2 + \frac{\alpha}{2}\left(\langle \log(\gamma^2 + (Hu-f)^2), \mathbf{1}\rangle + \mu\|Hu-u_0\|^2\right),$$

with a $\tau^{k+1} \in \partial H_k(u^{k+1})$ satisfying

$$\|\tau^{k+1}\| \le \frac{\rho\eta}{2}\|u^{k+1}-u^k\|, \quad (0<\eta<1).$$

2.3 Numerical algorithm

Since the $\varphi(\|d_i u\|)$ is nonconvex and nonsmooth with respect to u, it is usually difficult to solve. Here, we adopt the linearization technique to handle it. Given u^k, $\varphi(\|d_i u\|)$ is linearized at $\|d_i u^k\|$ by the first order Taylor approximation, and then we compute u^{k+1} by solving

$$(\mathcal{F}_k) \quad \min_{u\in\mathbb{R}^m} \; F_k(u) := \sum_{i\in J} \varphi'(\|d_i u^k\|)\|d_i u\| + \frac{\alpha}{2}\left(\langle \log(\gamma^2 + (Hu-f)^2), \mathbf{1}\rangle + \mu\|Hu-u_0\|^2\right).$$

For the optimization problem $(\mathcal{F}_k)$, we solve an inexact solution of it. Together with the proximal strategy, we propose the following algorithm.

For the inner optimization problem, we adopt ADMM [27, 35, 37] to handle it due to its good separable structure and strong convexity. Firstly, auxiliary variables p and v are introduced

$$\begin{aligned} &p_i = d_i u \quad \text{for } \forall i \in J, \\ &v = Hu. \end{aligned}$$

Consequently, u^{k+1} is solved by the following minimization

$$\min_{u,p,v} \; \sum_{i\in J} \varphi'(\|d_i u^k\|)\|p_i\| + \frac{\rho}{2}\|u-u^k\|^2 + \frac{\alpha}{2}\left(\langle \log(\gamma^2 + (v-f)^2), \mathbf{1}\rangle + \mu\|v-u_0\|^2\right), \tag{2.2a}$$

$$\text{s.t.} \quad p_i = d_i u, \quad \forall i \in J, \tag{2.2b}$$

$$v = Hu. \tag{2.2c}$$

Algorithm 2.2 ADMM: the alternating direction method of multipliers for solving u^{k+1}.

Step 0. Input u^k, α, λ, $\tilde{\lambda}$, r_1, r_2.
Initialize $u^{k,0}=u^k$, $p^{k,0}=0$, $v^{k,0}=0$, $\lambda^{k,0}=0$, $\tilde{\lambda}^{k,0}=0$.

Step 1. For $t=0,1,2,\cdots$, compute

$$\begin{cases} u^{k,t+1}\in\arg\min_u \mathscr{L}(u,p^{k,t},v^{k,t};\lambda^{k,t},\tilde{\lambda}^{k,t}); & \text{(2.3a)}\\ (p^{k,t+1},v^{k,t+1})\in\arg\min_{p,v} \mathscr{L}(u^{k,t+1},p,v;\lambda^{k,t},\tilde{\lambda}^{k,t}); & \text{(2.3b)}\\ \lambda_i^{k,t+1}=\lambda_i^{k,t}+r_1(d_iu^{k,t+1}-p_i^{k,t+1}),\ \forall i\in J; & \text{(2.3c)}\\ \tilde{\lambda}^{k,t+1}=\tilde{\lambda}^{k,t}+r_2(Hu^{k,t+1}-v^{k,t+1}). & \text{(2.3d)}\end{cases}$$

Step 2. If a termination criterion is not met, then go to Step 1. Otherwise, $u^{k+1}=u^{k,t+1}$.

The augmented Lagrangian functional for this optimization problem (2.2) writes

$$\begin{aligned}\mathscr{L}(u,p,v;\lambda,\tilde{\lambda})=&\sum_{i\in J}\varphi'(\|d_iu^k\|)\|p_i\|+\frac{\rho}{2}\|u-u^k\|^2\\&+\frac{\alpha}{2}\left(\langle\log(\gamma^2+(v-f)^2),\mathbf{1}\rangle+\mu\|v-u_0\|^2\right)+\sum_{i\in J}\langle\lambda_i,d_iu-p_i\rangle\\&+\frac{r_1}{2}\sum_{i\in J}\|d_iu-p_i\|^2+\langle\tilde{\lambda},Hu-v\rangle+\frac{r_2}{2}\|Hu-v\|^2,\end{aligned}$$

where λ, $\tilde{\lambda}$ are Lagrange multipliers, and r_1, r_2 are positive constants. The corresponding ADMM procedure is given as follows.

We now deal with each subproblem in the above ADMM.

• The u-subproblem (2.3a):

$$\begin{aligned}u^{k,t+1}\in\arg\min_u\Big\{&\sum_{i\in J}\langle\lambda_i^{k,t},d_iu\rangle+\frac{r_1}{2}\sum_{i\in J}\|d_iu-p_i^{k,t}\|^2+\frac{\rho}{2}\|u-u^k\|^2\\&+\langle\tilde{\lambda}^{k,t},Hu\rangle+\frac{r_2}{2}\|Hu-v^{k,t}\|^2\Big\}.\end{aligned}$$

The optimality condition for this least squares problem yields the following linear equation

$$(r_1D^*D+r_2H^*H+\rho I)u=D^*\left(r_1p^{k,t}-\lambda^{k,t}\right)+\rho u^k+H^*\left(r_2v^{k,t}-\tilde{\lambda}^{k,t}\right),\qquad(2.4)$$

where D^* and H^* are conjugate matrices of D and H. When we consider the periodic boundary condition in difference operators as shown in basic notation part, D^*D and

H^*H of (2.4) are all block circulant matrices which can be efficiently computed by the fast Fourier transform (FFT) as in [1,16,35,37,42]. Alternatively, the Neumann boundary condition is always used in difference operators [4, 22]. Together with the symmetric blurring kernel function, D^*D and H^*H are block Toeplitz-plus-Hankel matrices and the linear equation (2.4) can be solved by 2D discrete cosine transforms as that in [22]. In this paper, we conduct numerical experiments using the periodic boundary condition.

• The (p,v)-subproblem (2.3b): This problem is actually separable, where p, v can be computed parallel. In particular, p is calculated by

$$p^{k,t+1}\in\arg\min_p\left\{\sum_{i\in J}\varphi'(\|d_iu^k\|)\|p_i\|+\frac{r_1}{2}\sum_{i\in J}\left\|p_i-\left(d_iu^{k,t+1}+\frac{\lambda_i^{k,t}}{r_1}\right)\right\|^2\right\},$$

whose solution $p_i^{k,t+1}$ is

$$p_i^{k,t+1}=\text{shrink}\left(d_iu^{k,t+1}+\frac{\lambda_i^{k,t}}{r_1},\frac{\varphi'(\|d_iu^k\|)}{r_1}\right),\quad\forall i\in J,\tag{2.5}$$

with

$$\text{shrink}(a,b)=\frac{a}{\|a\|}*\max(\|a\|-b,0).$$

The v is computed by

$$\begin{aligned}v^{k,t+1}\in\arg\min_v\Bigg\{&\frac{\alpha}{2}\left(\langle\log(\gamma^2+(v-f)^2),\mathbf{1}\rangle+\mu\|v-u_0\|^2\right)\\&+\langle\tilde{\lambda}^{k,t},v\rangle+\frac{r_2}{2}\|Hu^{k,t+1}-v\|^2\Bigg\}.\end{aligned}$$

Let

$$G(v)=\frac{\alpha}{2}\left(\langle\log(\gamma^2+(v-f)^2),\mathbf{1}\rangle+\mu\|v-u_0\|^2\right)+\langle\tilde{\lambda}^{k,t},v\rangle+\frac{r_2}{2}\|Hu^{k,t+1}-v\|^2.$$

Similar to [21,30], v is obtained by Newton's mehtod

$$v^{k,t+1}=v^{k,t}-\frac{G'(v^{k,t})}{G''(v^{k,t})},\tag{2.6}$$

where G' and G'' are the gradient and Hessian matrices of G.

3 Convergence analysis

According to an abstract convergence result for descent methods in nonconvex analyses [3], we can prove the global convergence of $\{u^k\}$ in the proposed IIAPL for our

nonconvex Lipschitz model. The main goal is to verify a sufficient decrease property and a relative error tolerance property of the subdifferential when the objective function satisfies the Kurdyka-Łojasiewicz (KL) property. Firstly, we give the definition of the Kurdyka-Łojasiewicz (KL) property.

Definition 3.1 (Kurdyka-Łojasiewicz (KL) property [2]). *The function $h:\mathbb{R}^n\to(-\infty,+\infty]$ is said to have the Kurdyka-Łojasiewicz property at $\overline{x}\in\operatorname{dom}\partial h:=\{x\in\mathbb{R}^n:\partial h(x)\neq\emptyset\}$ if there exist $\gamma\in(0,+\infty]$, a neighborhood U of $\overline{x}$, and a continuous concave function $\phi\in\Phi_\gamma$, where Φ_γ stands for a class of function ϕ:*

(i) $\phi:[0,\gamma)\to(0,+\infty]$ *and* $\phi(0)=0$;

(ii) ϕ *is continuous differentiable on* $(0,\gamma)$;

(iii) for all $s\in(0,\gamma)$, $\phi'(s)>0$;

(iv) for all $x\in U\cap\{x\in\mathbb{R}^n:h(\overline{x})<h(x)<h(\overline{x})+\gamma\}$, *the Kurdyka-Łojasiewicz (KL) inequality holds:*

$$\phi'(h(x)-h(\overline{x}))dist(0,\partial h(x))\geq 1,$$

where $dist(0,\partial h(x))=\inf\{\|w\|:w\in\partial h(x)\}$.

If h satisfies the KL property at each point of $\operatorname{dom}\partial h$, *$h$ is called a KL function.*

Many KL functions have been used in practice applications [3, 6, 21, 43] such as real polynomial functions, logistic loss function, and indicator function of the positive semidefinite cone.

Secondly, the sufficient decrease property of the objective function is given in the following proposition.

Proposition 3.1 (Sufficient decrease property). *$\{F(u^k)\}$ is a nonincreasing sequence and satisfies*

$$\frac{\rho}{2}(1-\eta)\|u^{k+1}-u^k\|^2\leq F(u^k)-F(u^{k+1}),\quad\forall k\geq 0. \tag{3.1}$$

Moreover, the sequence $\{u^k\}$ satisfies

$$\lim_{k\to\infty}\|u^{k+1}-u^k\|=0.$$

Proof. Since $\varphi(t)$ is a concave function, we have

$$\varphi(\|d_iu\|)\leq\varphi(\|d_iu^k\|)+\varphi'(\|d_iu^k\|)(\|d_iu\|-\|d_iu^k\|),\quad\forall i\in J. \tag{3.2}$$

Then,

$$\begin{aligned}
&F(u^{k+1})+\frac{\rho}{2}\|u^{k+1}-u^k\|^2\\
=&\sum_{i\in J}\varphi(\|d_iu^{k+1}\|)+\frac{\rho}{2}\|u^{k+1}-u^k\|^2\\
&+\frac{\alpha}{2}\left(\langle\log(\gamma^2+(Hu^{k+1}-f)^2),\mathbf{1}\rangle+\mu\|Hu^{k+1}-u_0\|^2\right)\\
\leq&\sum_{i\in J}\Big(\varphi(\|d_iu^k\|)+\varphi'(\|d_iu^k\|)(\|d_iu^{k+1}\|-\|d_iu^k\|)\Big)+\frac{\rho}{2}\|u^{k+1}-u^k\|^2\\
&+\frac{\alpha}{2}\left(\langle\log(\gamma^2+(Hu^{k+1}-f)^2),\mathbf{1}\rangle+\mu\|Hu^{k+1}-u_0\|^2\right)\\
=&H_k(u^{k+1})+\sum_{i\in J}\Big(\varphi(\|d_iu^k\|)-\varphi'(\|d_iu^k\|)\|d_iu^k\|\Big)\\
\leq&H_k(u^k)-\langle\tau^{k+1},u^k-u^{k+1}\rangle+\sum_{i\in J}\Big(\varphi(\|d_iu^k\|)-\varphi'(\|d_iu^k\|)\|d_iu^k\|\Big)\\
=&F(u^k)-\langle\tau^{k+1},u^k-u^{k+1}\rangle\\
\leq&F(u^k)+\frac{\rho\eta}{2}\|u^{k+1}-u^k\|^2,
\end{aligned}\tag{3.3}$$

where the first equality is from (3.2) and the second equality is based on the convexity of $H_k(u)$. Obviously, (3.3) implies (3.1). Moreover, because the sequence $\{F(u^k)\}$ is bounded, and thus $\{F(u^k)\}$ is convergent. This also indicates $\lim_{k\to\infty}\|u^{k+1}-u^k\|=0$. □

Next, we show the relative error property of the subdifferential of $F(u)$ in (2.1).

Proposition 3.2 (Relative error property)**.** *Suppose that $F(u)$ is the objective function in the model* (2.1) *and $\{u^k\}$ is the generated sequence by IIAPL. Then, there exists a $\vartheta^{k+1}\in\partial F(u^{k+1})$ such that*

$$\|\vartheta^{k+1}\|\leq\left(\sum_{i\in J}L\|d_i\|^2+\rho+\frac{\rho\eta}{2}\right)\|u^{k+1}-u^k\|,\tag{3.4}$$

where L is the Lipschitz gradient constant of $\varphi(t)$ defined in Assumption 2.1(b)*, and ρ, η are two constants defined in the proposed IIAPL algorithm.*

Proof. From [28, Exercise 8.8], [28, Corollary 10.9] and [13, Proposition 4] that

$$\begin{aligned}
\partial F(u^{k+1})=&\sum_{i\in J}\varphi'(\|d_iu^{k+1}\|)(d_i)^T\mathrm{sign}(d_iu^{k+1})\\
&+\alpha\left(\frac{H^T(Hu^{k+1}-f)}{\gamma^2+(Hu^{k+1}-f)^2}+\mu H^T(Hu^{k+1}-u_0)\right),
\end{aligned}\tag{3.5}$$

where

$$\operatorname{sign}(d_i u^{k+1}) = \begin{cases} \dfrac{d_i u^{k+1}}{\|d_i u^{k+1}\|}, & \|d_i u^{k+1}\| \neq 0, \\ \{\iota_i^{k+1} : \|\iota_i^{k+1}\| \leq 1,\ \iota_i^{k+1} \in \mathbb{R}^2\}, & \|d_i u^{k+1}\| = 0. \end{cases}$$

Moreover, $\tau^{k+1} \in \partial H_k(u^{k+1})$ in our algorithm IIAPL gives

$$\begin{aligned} \tau^{k+1} \in \partial H_k(u^{k+1}) = \sum_{i \in J} \varphi'(\|d_i u^k\|)(d_i)^T \operatorname{sign}(d_i u^{k+1}) + \rho(u^{k+1} - u^k) \\ + \alpha \left(\frac{H^T(Hu^{k+1} - f)}{\gamma^2 + (Hu^{k+1} - f)^2} + \mu H^T(Hu^{k+1} - u_0) \right). \end{aligned}$$

Assume that there exists a $\iota_i^{k+1} \in \mathbb{R}^2$ with $\|\iota_i^{k+1}\| \leq 1$ in the above equality such that

$$\begin{aligned} \tau^{k+1} = \sum_{i \in \Omega_0^{k+1}} \varphi'(\|d_i u^k\|)(d_i)^T \iota_i^{k+1} + \sum_{i \in \Omega_1^{k+1}} \varphi'(\|d_i u^k\|) \frac{(d_i)^T d_i u^{k+1}}{\|d_i u^{k+1}\|} + \rho(u^{k+1} - u^k) \\ + \alpha \left(\frac{H^T(Hu^{k+1} - f)}{\gamma^2 + (Hu^{k+1} - f)^2} + \mu H^T(Hu^{k+1} - u_0) \right), \end{aligned} \tag{3.6}$$

where $\Omega_0^{k+1} = \{i \in J : \|d_i u^{k+1}\| = 0\}$ and $\Omega_1^{k+1} = \{i \in J : \|d_i u^{k+1}\| \neq 0\}$. Similarly, in (3.5), there exists a $\vartheta^{k+1} \in \partial F(u^{k+1})$ with the above $\iota_i^{k+1} \in \mathbb{R}^2$ with $\|\iota_i^{k+1}\| \leq 1$ such that

$$\begin{aligned} \vartheta^{k+1} = \sum_{i \in \Omega_0^{k+1}} \varphi'(\|d_i u^{k+1}\|)(d_i)^T \iota_i^{k+1} + \sum_{i \in \Omega_1^{k+1}} \varphi'(\|d_i u^{k+1}\|) \frac{(d_i)^T d_i u^{k+1}}{\|d_i u^{k+1}\|} \\ + \alpha \left(\frac{H^T(Hu^{k+1} - f)}{\gamma^2 + (Hu^{k+1} - f)^2} + \mu H^T(Hu^{k+1} - u_0) \right). \end{aligned} \tag{3.7}$$

Combining (3.6) and (3.7) implies

$$\begin{aligned} \vartheta^{k+1} - \tau^{k+1} = \sum_{i \in \Omega_0^{k+1}} (\varphi'(\|d_i u^{k+1}\|) - \varphi'(\|d_i u^k\|))(d_i)^T \iota_i^{k+1} \\ + \sum_{i \in \Omega_1^{k+1}} \left((\varphi'(\|d_i u^{k+1}\|) - \varphi'(\|d_i u^k\|)) \frac{(d_i)^T d_i u^{k+1}}{\|d_i u^{k+1}\|} \right) - \rho(u^{k+1} - u^k). \end{aligned}$$

Then, we get

$$\begin{aligned}\|\vartheta^{k+1}-\tau^{k+1}\| &\le \sum_{i\in\Omega_0^{k+1}} |\varphi'(\|d_iu^{k+1}\|)-\varphi'(\|d_iu^k\|)|\|d_i\| \\ &\quad+\sum_{i\in\Omega_1^{k+1}}\left(|\varphi'(\|d_iu^{k+1}\|)-\varphi'(\|d_iu^k\|)|\frac{\|d_i\|\|d_iu^{k+1}\|}{\|d_iu^{k+1}\|}\right)+\rho\|u^{k+1}-u^k\| \\ &\le \sum_{i\in\Omega_0^{k+1}} L\|d_i\|^2\|u^{k+1}-u^k\|+\sum_{i\in\Omega_1^{k+1}} L\|d_i\|^2\|u^{k+1}-u^k\|+\rho\|u^{k+1}-u^k\| \\ &= \left(\sum_{i\in J} L\|d_i\|^2+\rho\right)\|u^{k+1}-u^k\|,\end{aligned}$$

where the second inequality is from Assumption 2.1(b). Together with

$$\|\tau^{k+1}\|\le\frac{\rho\eta}{2}\|u^{k+1}-u^k\|$$

in our algorithm IIAPL, we have $\vartheta^{k+1}\in\partial F(u^{k+1})$ satisfying

$$\begin{aligned}\|\vartheta^{k+1}\| &\le \|\tau^{k+1}\|+\left(\sum_{i\in J} L\|d_i\|^2+\rho\right)\|u^{k+1}-u^k\| \\ &\le \left(\sum_{i\in J} L\|d_i\|^2+\rho+\frac{\rho\eta}{2}\right)\|u^{k+1}-u^k\|.\end{aligned}$$

This completes the proof. □

The global convergence of $\{u^k\}$ is given as follows.

Theorem 3.1 (Global convergence)**.** *Suppose that the objective function $F(u)$ in* (2.1) *satisfies the KL property. Let $\{u^k\}$ be a sequence generated by IIAPL. Then $\{u^k\}$ converges to a critical point u^* of the original function $F(u)$.*

Proof. Since $F(u)$ is coercive and the sequence $\{F(u^k)\}$ is bounded from Proposition 3.1, $\{u^k\}$ is bounded. Then, there exists a convergent subsequence $\{u^{k_j}\}$ such that $\{u^{k_j}\}\to\widetilde{u}$ and $\{F(u^{k_j})\}\to F(\widetilde{u})$ as $j\to\infty$. Combining (3.1), (3.4) and by [3, Theorem 2.9], the sequence $\{u^k\}$ converges to $u^*=\widetilde{u}$, which implies that u^* is a critical point of $F(u)$. □

4 Experimental results

In this section, we mainly investigate the performance of our first-order nonconvex regularization model with the proposed algorithm compared to the Median filter, the first-order convex TV method [30] and the nonconvex regularization with the nonconvex fidelity term model [1] for deblurring images under Cauchy moise. For simplicity, the

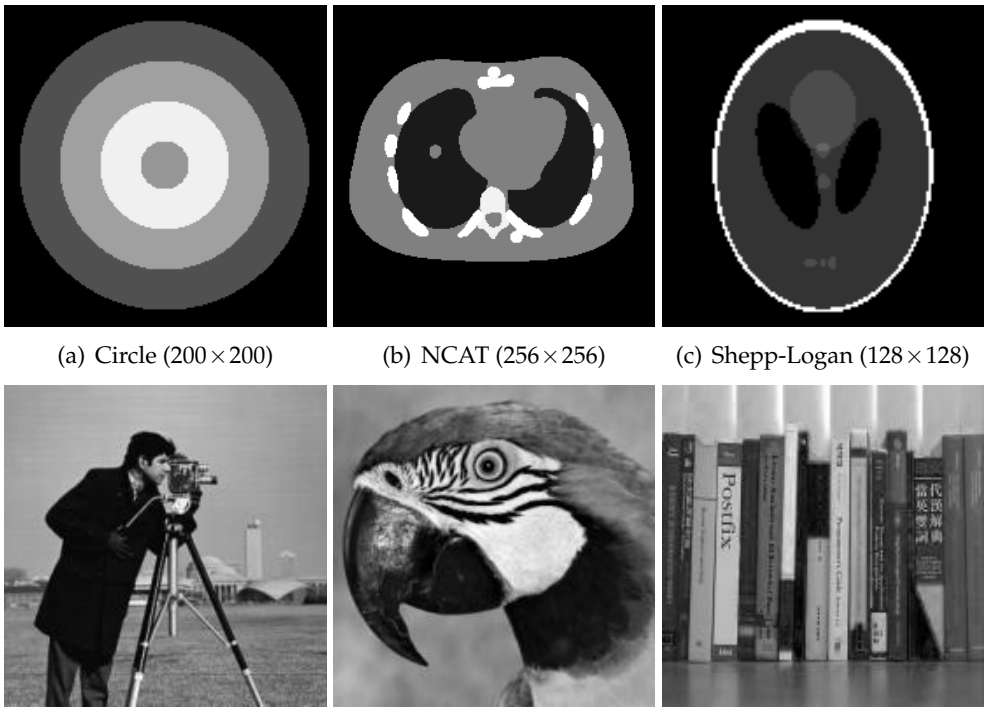

(a) Circle (200×200) (b) NCAT (256×256) (c) Shepp-Logan (128×128)

(d) Cameraman (256×256) (e) Parrot (256×256) (f) Books (704×576)

Figure 2: Test images.

models in [30] and [1] are respectively denoted as TV and NN. All numerical experiments are conducted using Windows 10 and MATLAB R2019b on a desktop with the Intel i5-10400f processor at 4.3GHz and 16G RAM. Except for the visual quality evaluation, we also use the peak signal-to-noise ratio (PSNR) and the structural similarity (SSIM) [36] as two quantitative indexes.

Fig. 2 shows six test images, where pixel values of images are all scaled to the interval [0,1]. Four types of blurring kernels are tested: type 1 (**fspecial ('average',9)**), type 2 (**fspecial ('motion',15,30)**), type 3 (**fspecial ('gaussian',[9,9],10)**) and type 4 (**fspecial ('disk',4)**). In all experiments, we generate the blurred images with Cauchy noise by using the following degradation

$$f = Hu + \xi \frac{\eta_1}{\eta_2},$$

where H is a linear blur matrix, $\xi > 0$ denotes the noise level, η_1 and η_2 are independent random variables following Gaussian distribution with mean 0 and variation 1.

In IIAPL, there are two loops. The inner loop is terminated when $\frac{\|u^{k,t+1}-u^{k,t}\|}{\|u^{k,t+1}\|} < 10^{-4}$ or the number of inner iterations exceeds 20, while the termination criterion in the outer

loop is $\frac{|F(u^{k+1})-F(u^k)|}{|F(u^{k+1})|}<10^{-5}$. For the compared TV [30], we implement it by ADMM and use the same stopping condition $\frac{|F(u^{k+1})-F(u^k)|}{|F(u^{k+1})|}<10^{-5}$. For the NN method [1], we use the code from the authors and four parameters $\lambda,\alpha,\mu_1,\mu_2$ are tuned as that in [1]. In our model, the nonconvex potential function $\varphi(t)=\ln(1+at)$ is adopted, algorithm parameters are simply set as $r_1=10$, $r_2=10$, $\rho=10^{-4}$, and α,a are tuned to get the best PSNR values. For a fair comparison, we similarly let $r_1=10$, $r_2=10$, and choose the best parameter α in TV method. Moreover, to satisfy the convexity condition, all experiments are conducted under $8\mu\gamma^2=1$ as that in [30].

Fig. 3 shows different restorations by four methods for six test images which are corrupted by type 1 (**fspecial ('average',9)**) blurring kernel and Cauchy noise with $\xi=0.02$. One can see that the Median filter can remove most noises but has little effect on the blur. In contrast, other three methods are able to eliminate both noises and blur. However, our method can produce neater edges than TV [30] and NN [1] from the first and second rows in Fig. 3. Moreover, one can found that our model with the proposed algorithm is more suitable to remove blur and noise from images with more piecewise constant regions and higher contrasts. More restorations are presented in Figs. 4 and 5 when all test images are corrupted by type 2 (**fspecial ('motion',15,30)**) and type 4 (**fspecial('disk',4)**) blurring kernels and Cauchy noise with $\xi=0.02$. Figs. 6 and 7 give restored results by different methods for all test images corrupted by two different blurs and Cauchy noise with $\xi=0.04$. Similar phenomena can be observed as above, where our method yields more flat piecewise constant regions and neater edges because of the nonconvexity of regularization term in the proposed model. Tables 1 and 2 list more results on the PSNR, SSIM values and the computation time in seconds by different methods for images with different blurring kernels and Cauchy noise, where the best results are shown in bold. Although the running time of our method is a bit longer than Median filter and TV because of two loops in IIAPL, it achieves the best PSNR values on average.

Fig. 8 shows both $F(u^k)$ and $\|u^{k+1}-u^k\|$ versus the outer iteration number for "NCAT" and "Cameraman" under type 2 (**fspecial ('motion',15,30)**) blurring kernel and Cauchy noise with $\xi=0.02$. One can easily observe that the objective values and the iterative errors are decreasing as the iteration number increases. Except for the theoretical convergent result in Theorem 3.1, Fig. 8 verifies the convergence of our algorithm from the numerical viewpoint. To further observe the objective values of $H_k(u^{k,t})$ versus the last inner iteration number for "NCAT" and "Cameraman" in Fig. 8, Fig. 9 gives the curves. In the two cases, the inner iterations are terminated when the number of inner iterations exceeds 20. Since the solution of the v-subproblem in ADMM for solving the inner optimization problem is inexact, the objective values increases a little from the first iteration to the second iteration. However, it decreases after 2 iterations.

Moreover, some experimental results are presented for removing Cauchy noise only. Here, two recent methods [17,31] are compared, where [31] utilized the nonlinear diffusion equations and [17] adopted the weighted nuclear norm minimization strategy based on the nonlocal similarity of images. For simplicity, we respectively denote the mod-

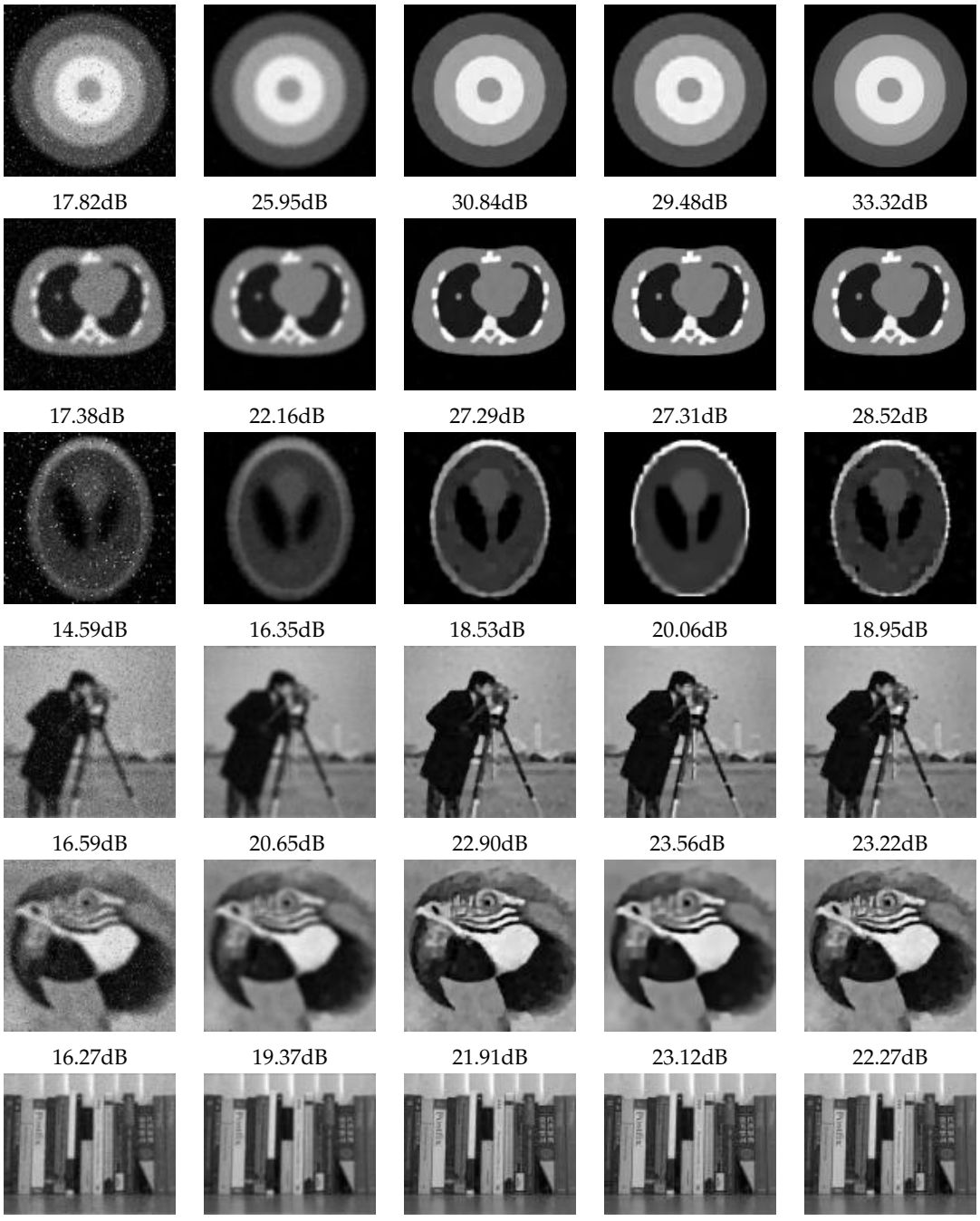

Figure 3: The first column: observed images corrupted by type 1 (**fspecial ('average',9)**) blurring kernel and Cauchy noise with $\xi=0.02$. From the second column to the fifth column: restored images by Median filter, TV, NN and our method. PSNR values are also listed.

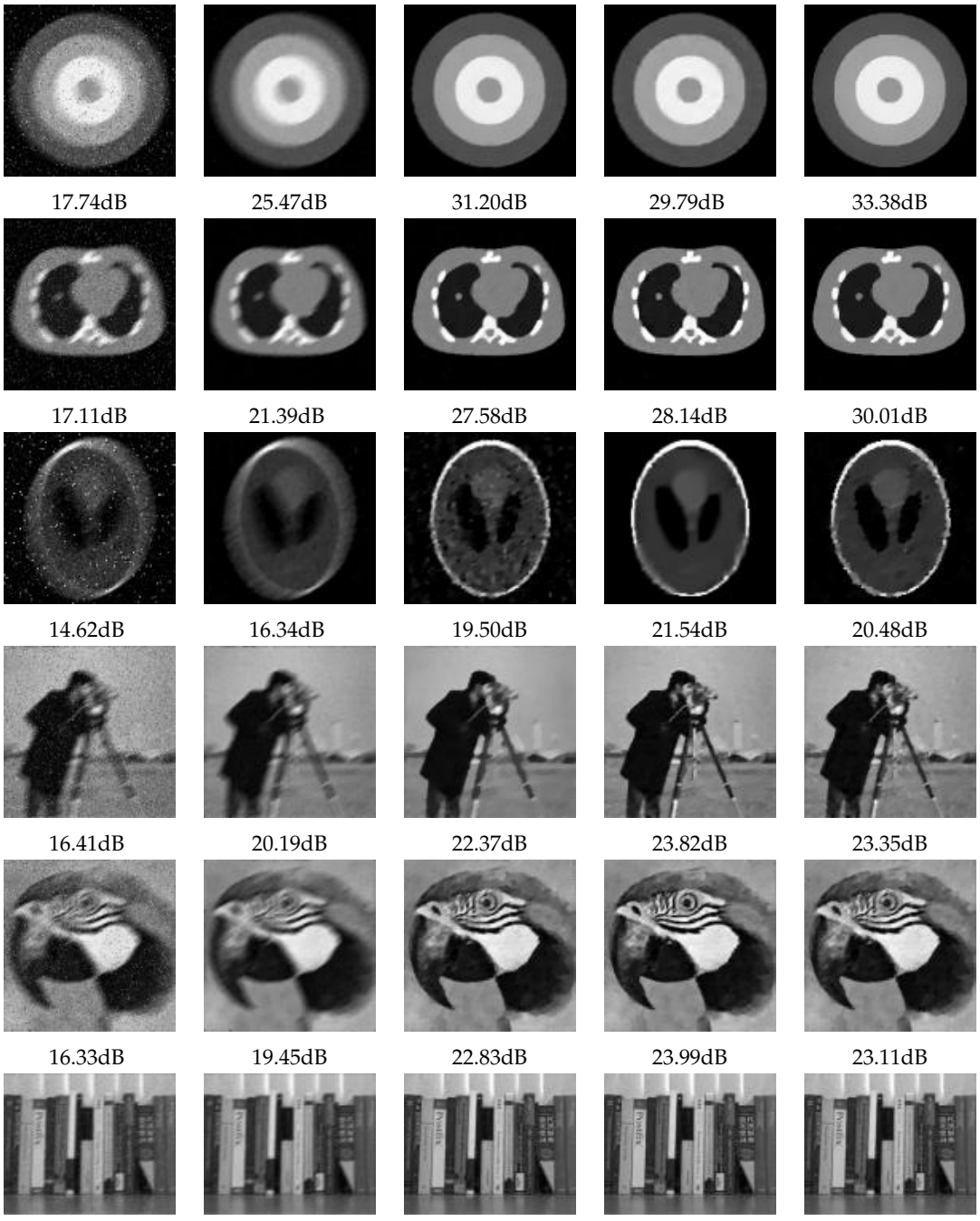

Figure 4: The first column: observed images corrupted by type 2 (**fspecial ('motion',15,30)**) blurring kernel and Cauchy noise with $\xi=0.02$. From the second column to the fifth column: restored images by Median filter, TV, NN and our method. PSNR values are also listed.

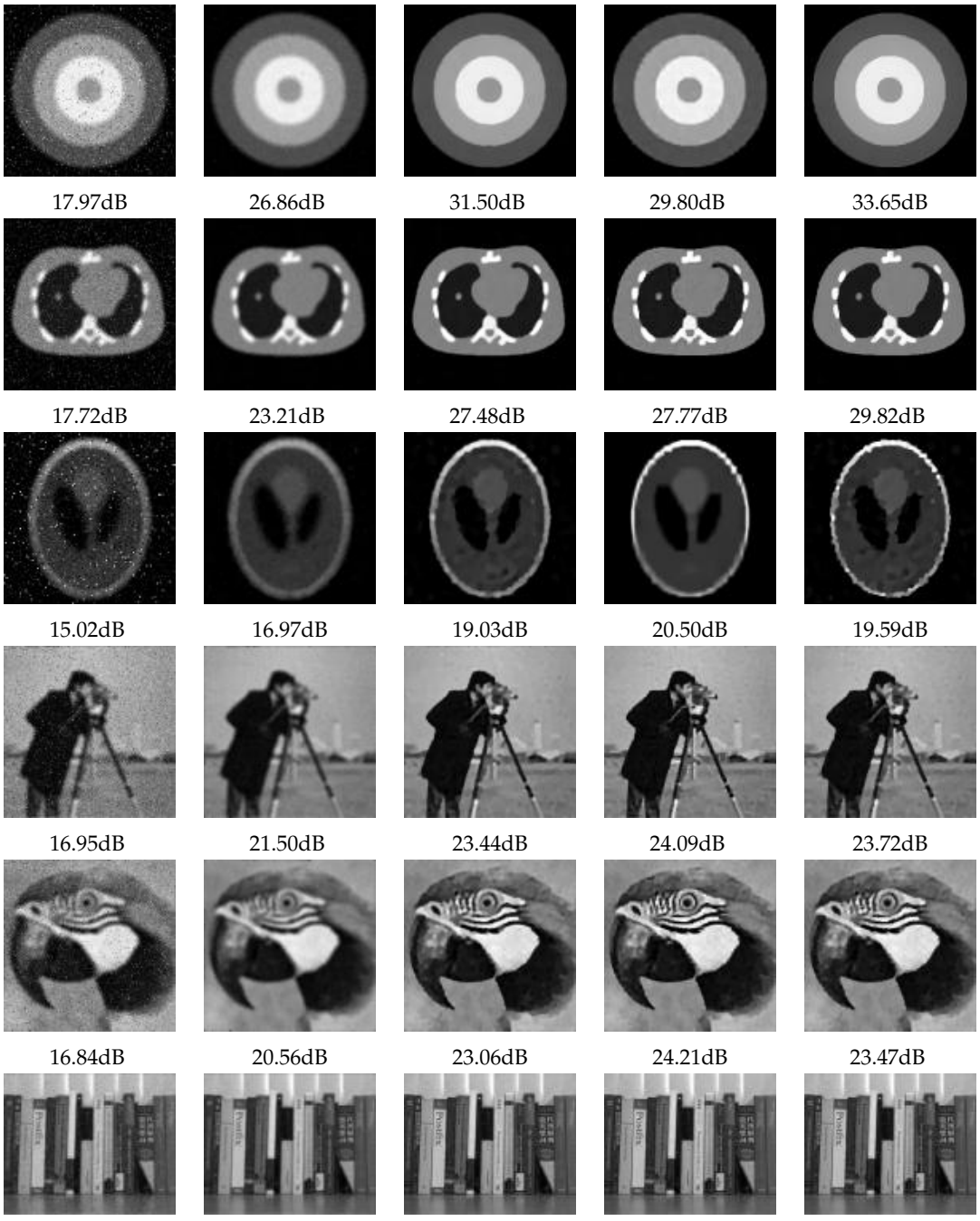

Figure 5: The first column: observed images corrupted by type 4 (**fspecial('disk',4)**) blurring kernel and Cauchy noise with $\xi = 0.02$. From the second column to the fifth column: restored images by Median filter, TV, NN and our method. PSNR values are also listed.

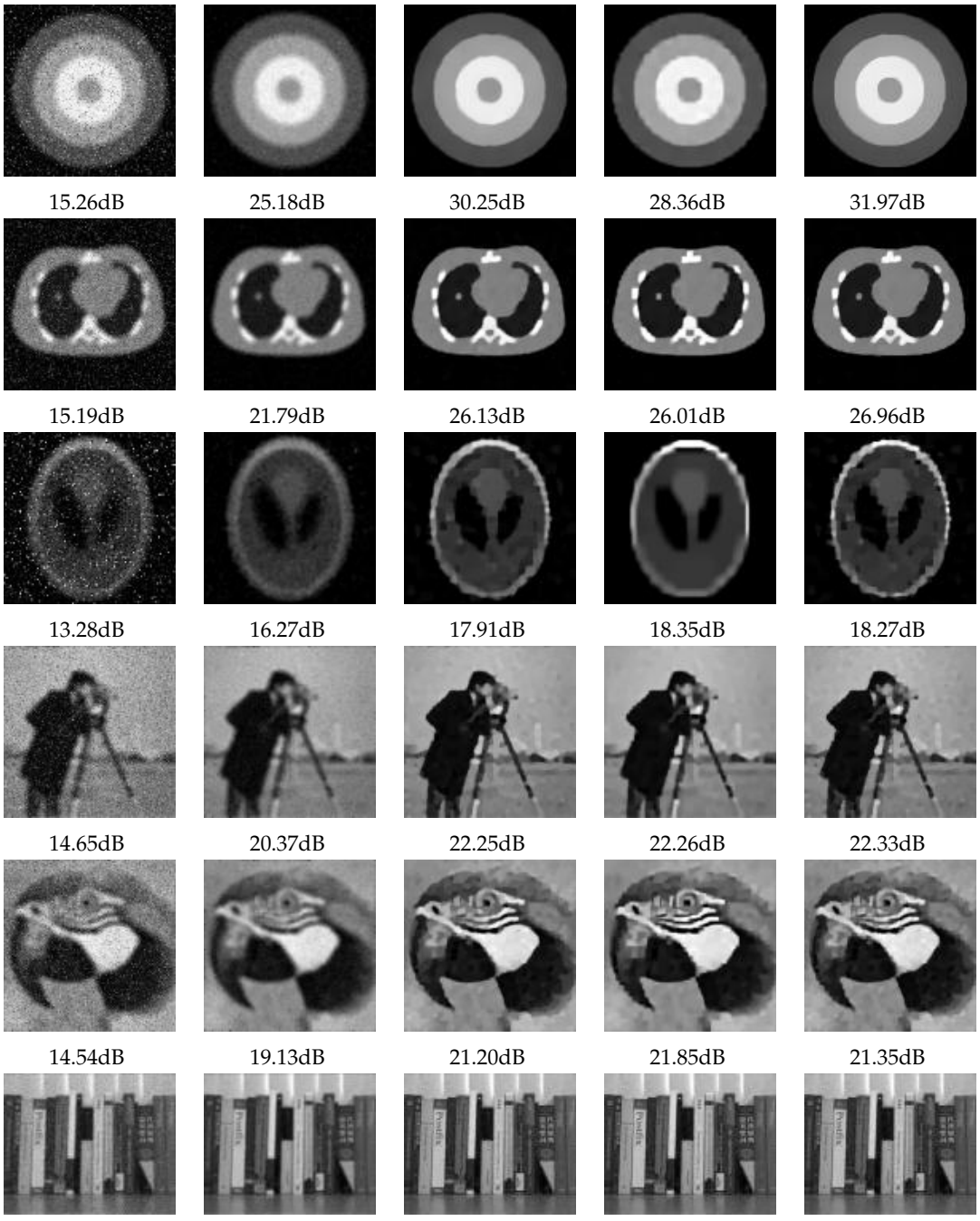

Figure 6: The first column: observed images corrupted by type 1 (**fspecial ('average',9)**) blurring kernel and Cauchy noise with $\xi=0.04$. From the second column to the fifth column: restored images by Median filter, TV, NN and our method. PSNR values are also listed.

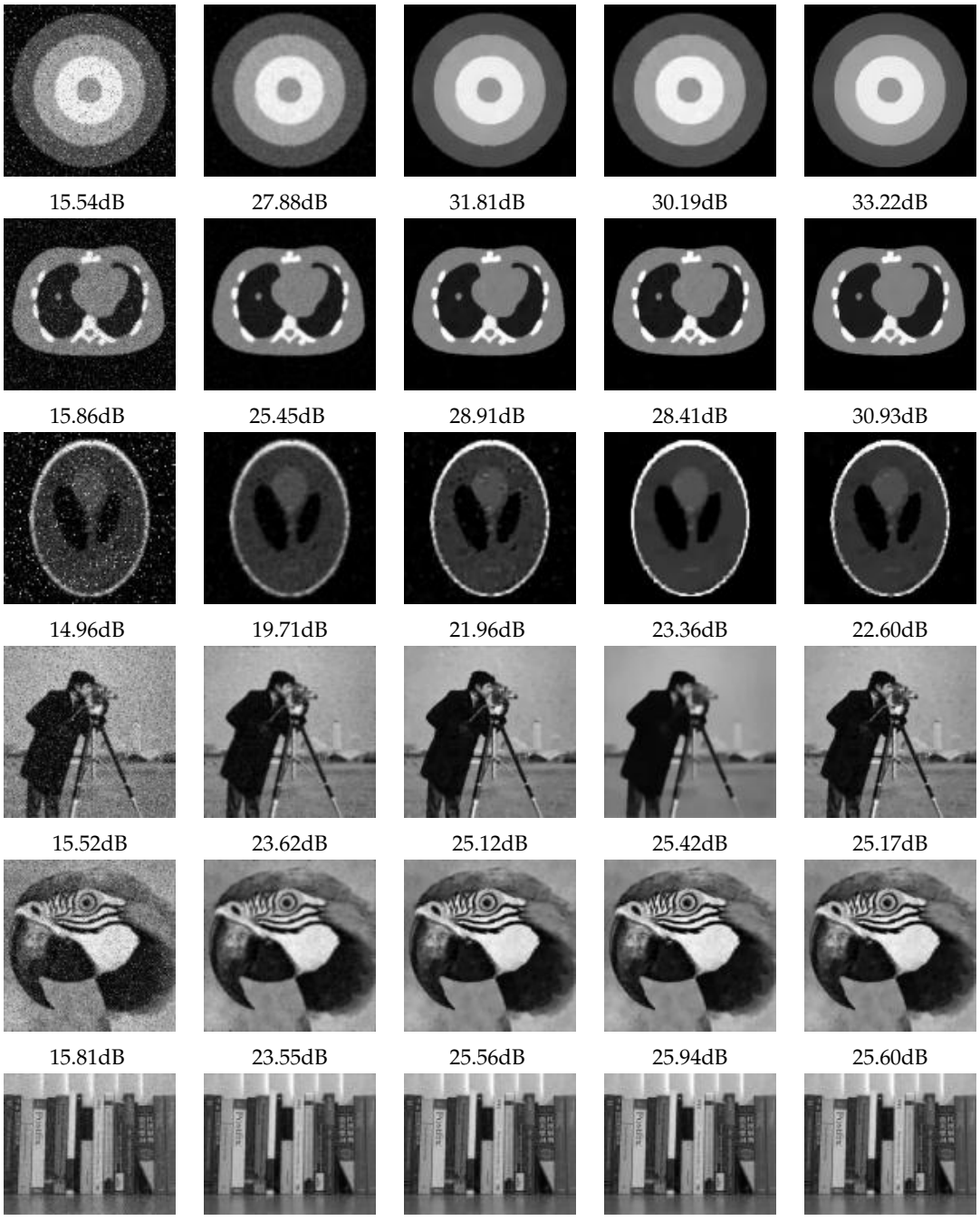

Figure 7: The first column: observed images corrupted by type 3 (**fspecial ('gaussian',[9,9],10)**) blurring kernel and Cauchy noise with $\xi=0.04$. From the second column to the fifth column: restored images by Median filter, TV, NN and our method. PSNR values are also listed.

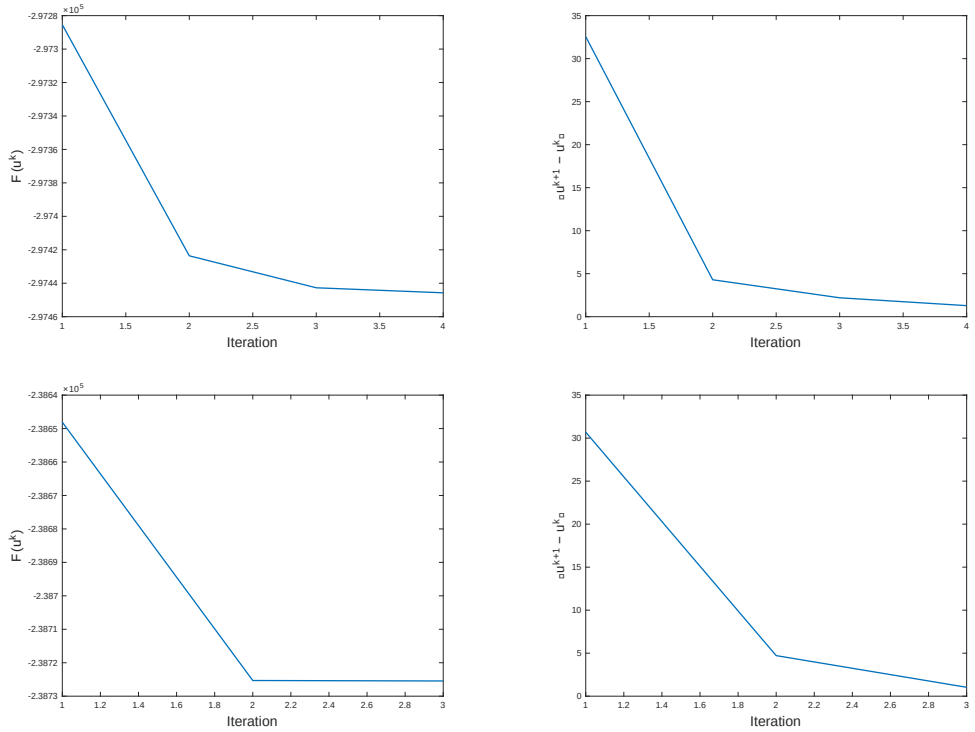

$F(u^k)$ versus the outer iteration number $\|u^{k+1}-u^k\|$ versus the outer iteration number

Figure 8: $F(u^k)$ and $\|u^{k+1}-u^k\|$ versus the outer iteration number for "NCAT" and "Cameraman" corrupted by type 2 (**fspecial ('motion',15,30)**) blurring kernel and Cauchy noise with $\xi=0.02$.

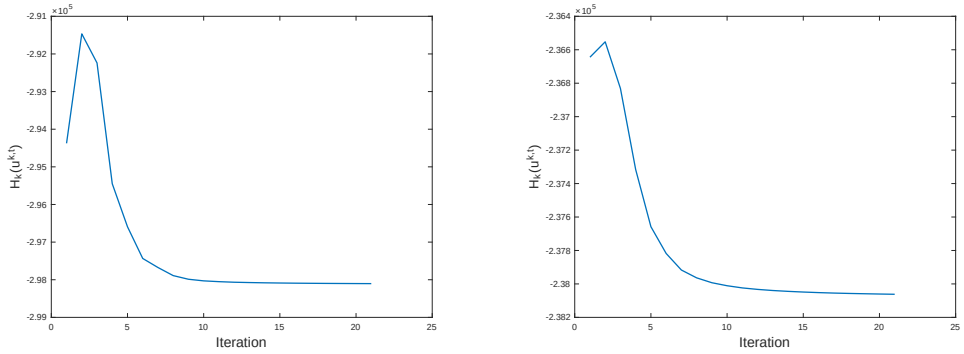

Figure 9: $H_k(u^{k,t})$ versus the last inner iteration number for "NCAT" (left) and "Cameraman" (right) corrupted by type 2 (**fspecial ('motion',15,30)**) blurring kernel and Cauchy noise with $\xi=0.02$.

Table 1: PSNR, SSIM and Time using different methods for images corrupted by four blurring kernels and Cauchy noise with $\xi = 0.02$.

Blur type	Image	Median filter PSNR/SSIM/Time	TV PSNR/SSIM/Time	NN PSNR/SSIM/Time	Our PSNR/SSIM/Time
average	Circle	25.95/0.6804/**0.03**	30.84/0.8883/0.12	29.48/0.9071/2.33	**33.32**/**0.9421**/0.50
	NCAT	22.16/0.6648/**0.03**	27.29/0.8709/0.19	27.31/**0.9234**/7.03	**28.52**/0.9174/0.65
	Shepp-Logan	16.35/0.5382/**0.03**	18.53/0.6360/0.10	**20.06**/**0.8315**/12.81	18.95/0.6025/0.22
	Cameraman	20.65/0.5615/**0.03**	22.90/0.6852/0.20	**23.56**/**0.7294**/3.64	23.22/0.7008/0.66
	Parrot	19.37/0.5887/**0.03**	21.91/0.6879/0.22	**23.12**/**0.7375**/11.13	22.27/0.7006/0.63
	Books	21.57/0.6125/**0.04**	23.58/0.7350/1.53	**25.00**/**0.7900**/17.23	24.05/0.7356/6.04
motion	Circle	25.47/0.6707/**0.03**	31.20/0.9113/0.11	29.79/0.9047/1.52	**33.38**/**0.9432**/0.46
	NCAT	21.39/0.6569/**0.03**	27.58/0.8511/0.20	28.14/0.8882/6.03	**30.01**/**0.9240**/0.84
	Shepp-Logan	16.34/0.5212/**0.03**	19.50/0.3775/0.13	**21.54**/**0.8670**/12.27	20.48/0.6747/0.27
	Cameraman	20.19/0.5613/**0.03**	22.37/0.6924/0.18	**23.82**/**0.6959**/4.96	23.35/0.6922/0.63
	Parrot	19.45/0.5986/**0.03**	22.83/0.7148/0.21	**23.99**/**0.7379**/6.28	23.11/0.7153/0.61
	Books	21.18/0.5406/**0.05**	23.58/0.7112/1.73	**24.76**/**0.7283**/18.47	23.91/0.7086/1.43
gaussian	Circle	29.81/0.8006/**0.03**	33.40/0.9311/0.10	31.62/0.9356/1.99	**35.37**/**0.9575**/0.49
	NCAT	26.66/0.7783/**0.03**	30.62/0.9041/0.19	30.06/0.9243/4.88	**33.57**/**0.9441**/0.85
	Shepp-Logan	20.15/0.7342/**0.04**	23.56/0.7394/0.10	**26.19**/**0.9145**/7.55	24.17/0.7933/0.23
	Cameraman	24.47/0.7355/**0.03**	26.26/0.7934/0.22	**26.86**/**0.8118**/2.08	26.38/0.7867/0.66
	Parrot	24.50/0.7795/**0.03**	26.98/0.8223/0.20	**27.47**/**0.8404**/2.78	27.08/0.8213/0.67
	Books	25.39/0.7926/**0.04**	27.32/0.8305/1.65	**28.80**/**0.8702**/15.37	27.56/0.8240/5.80
disk	Circle	26.86/0.7165/**0.03**	31.50/0.9226/0.13	29.80/0.9086/1.39	**33.65**/**0.9440**/0.48
	NCAT	23.21/0.6988/**0.03**	27.48/0.8897/0.14	27.77/0.9152/10.82	**29.82**/**0.9311**/0.84
	Shepp-Logan	16.97/0.5874/**0.03**	19.03/0.6128/0.09	**20.50**/**0.8543**/17.31	19.59/0.6327/0.70
	Cameraman	21.50/0.6030/**0.03**	23.44/0.7106/0.20	**24.09**/**0.7390**/4.08	23.72/0.7145/0.64
	Parrot	20.56/0.6410/**0.03**	23.06/0.7281/0.20	**24.21**/**0.7606**/9.65	23.47/0.7352/0.67
	Books	22.38/0.6621/**0.04**	23.84/0.7397/1.69	**24.95**/**0.7751**/19.26	24.12/0.7484/5.82
Average values		22.19/0.6552/**0.03**	25.36/0.7661/0.41	25.95/**0.8300**/8.37	**26.38**/0.7954/1.46

els in [31] and [17] as NDE and WNNM. As discussed in [31], two parameters α and σ of NDE are adjusted to obtain the best denoising performance, while all parameters of WNNM are fixed except for λ in [17]. In our method, we still use the nonconvex potential function $\varphi(t) = \ln(1+at)$, fix algorithm parameters $r_1 = 10$, $r_2 = 10$, $\rho = 10^{-4}$ and tune α, a. Figs. 10 and 11 illustrate the denoising results for test images corrupted by Cauchy noise with $\xi = 0.02$ and $\xi = 0.04$. Although the WNNM gets better restorations because of nonlocal similarity in most cases, our model with the proposed algorithm is able to achieve good performance with the least computation time among all compared methods as shown in Table 3.

5 Conclusions

In this paper, we introduced a nonconvex and nonsmooth model for blurred image restoration under Cauchy noise. It had the advantages of nonconvex Lipschitz regularization for preserving edges, as well as the data fidelity term for removing Cauchy noise. By the proximal linearization strategy, our nonconvex model was converted into a series of convex models, where these convex problems can be solved by ADMM. Based on an abstract convergence result for descent methods, the proposed algorithm was analyzed to

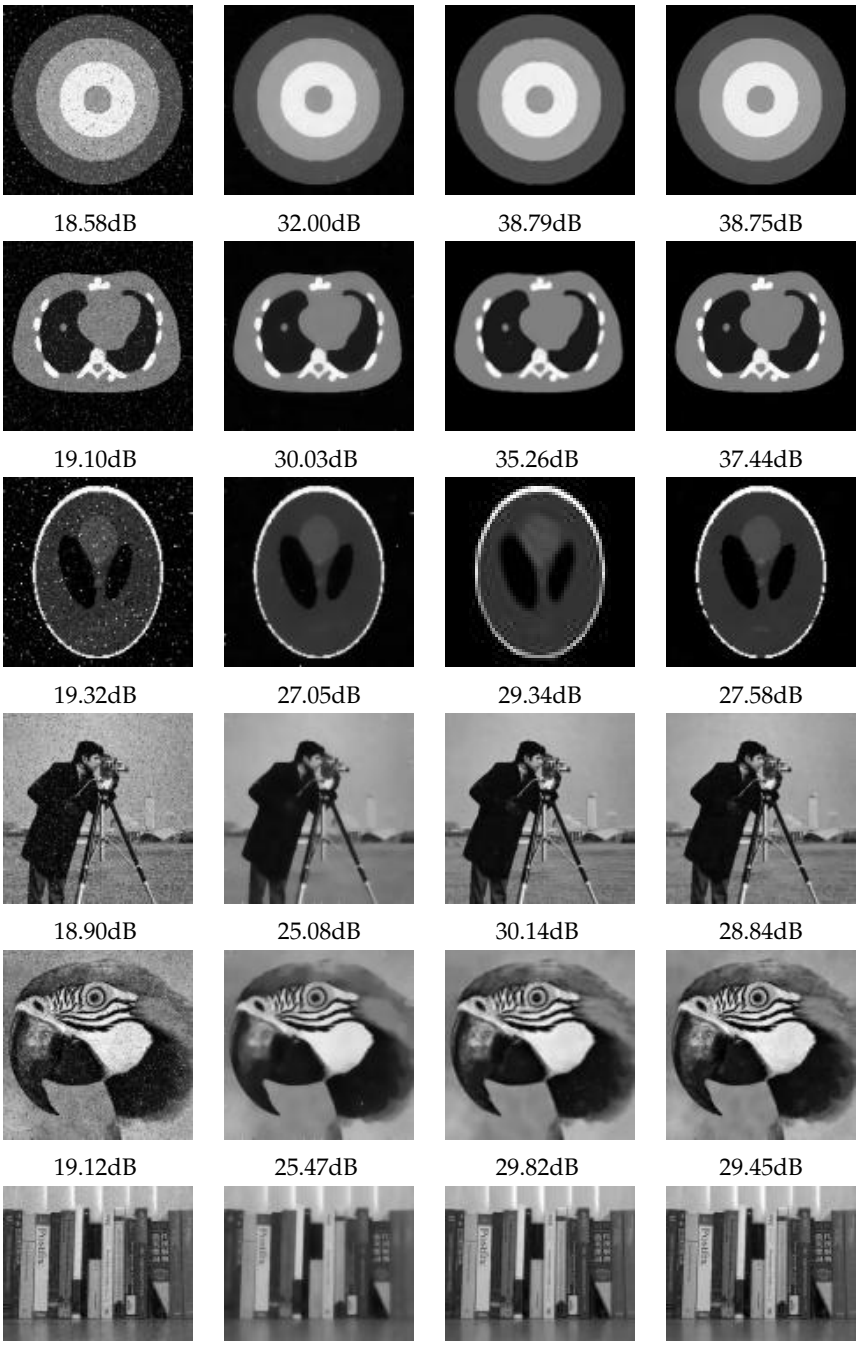

Figure 10: The first column: observed images corrupted by Cauchy noise with $\xi=0.02$. From the second column to the fourth column: restorations by NDE, WNNM and our method. PSNR values are also listed.

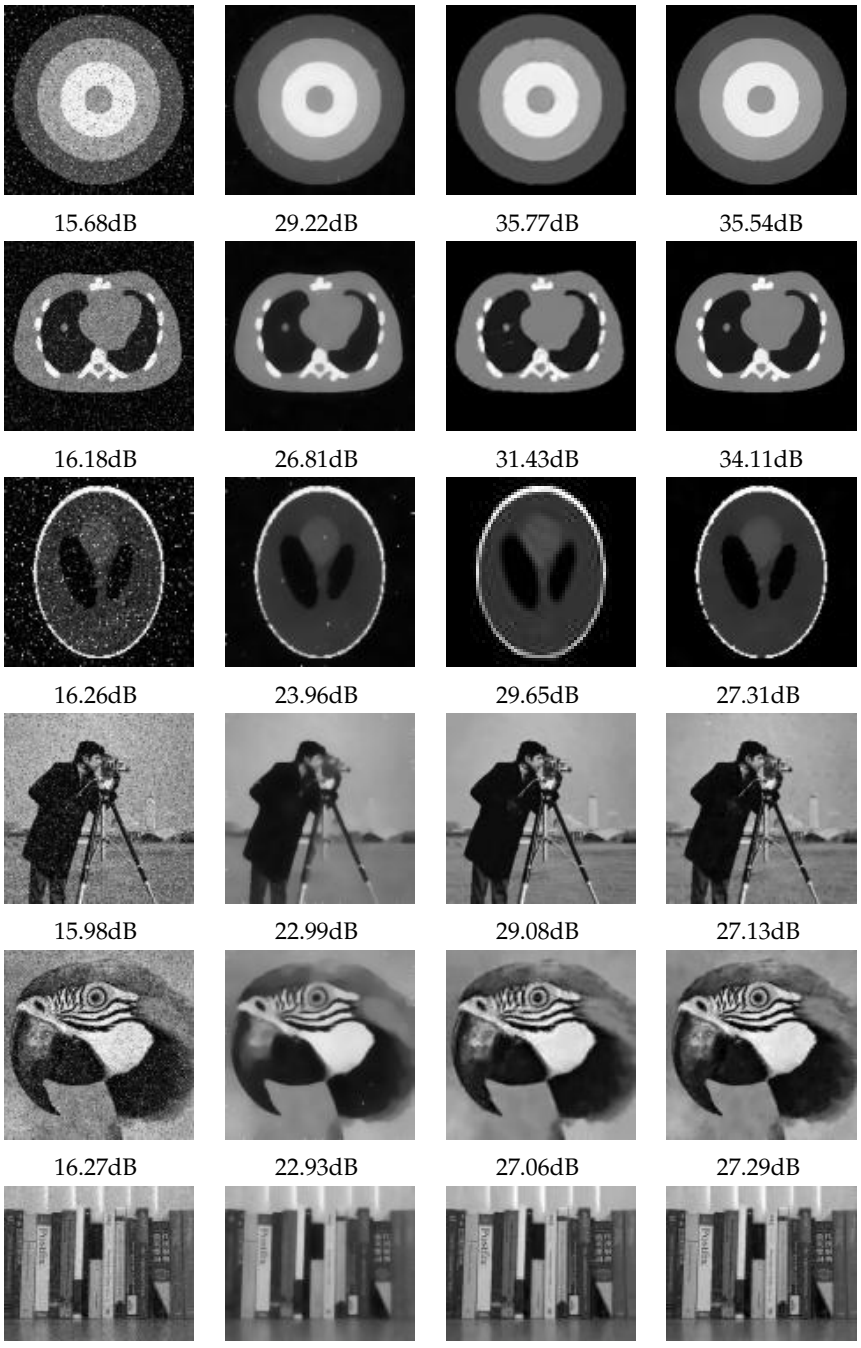

Figure 11: The first column: observed images corrupted by Cauchy noise with $\xi=0.04$. From the second column to the fourth column: restorations by NDE, WNNM and our method. PSNR values are also listed.

Table 2: PSNR, SSIM and Time using different methods for images corrupted by four blurring kernels and Cauchy noise with $\xi = 0.04$.

Blur type	Image	Median filter PSNR/SSIM/Time	TV PSNR/SSIM/Time	NN PSNR/SSIM/Time	Our PSNR/SSIM/Time
average	Circle	25.18/0.5160/**0.03**	30.25/0.8824/0.12	28.36/0.8855/1.85	**31.97**/**0.9043**/0.55
	NCAT	21.79/0.4756/**0.03**	26.13/0.8025/0.17	26.01/**0.9023**/7.00	**26.96**/0.8618/0.66
	Shepp-Logan	16.27/0.3914/**0.03**	17.91/0.5011/0.08	**18.35**/**0.7558**/17.46	18.27/0.5213/0.22
	Cameraman	20.37/0.4571/**0.03**	22.25/0.6647/0.17	22.26/**0.6900**/3.88	**22.33**/0.6640/0.64
	Parrot	19.13/0.4915/**0.03**	21.20/0.6623/0.20	**21.85**/**0.6943**/14.02	21.35/0.6602/0.63
	Books	21.26/0.5008/**0.04**	22.95/0.6904/1.49	**23.73**/**0.7405**/20.36	23.07/0.6925/5.79
motion	Circle	24.77/0.5094/**0.03**	30.16/0.8788/0.13	28.67/0.8916/2.32	**31.44**/**0.8919**/0.57
	NCAT	21.07/0.4687/**0.03**	25.75/0.7758/0.14	26.51/**0.8914**/12.03	**26.78**/0.8393/0.80
	Shepp-Logan	16.24/0.3817/**0.03**	18.42/0.4462/0.09	18.40/**0.7476**/14.57	**19.00**/0.5079/0.28
	Cameraman	19.93/0.4571/**0.03**	22.13/0.6530/0.19	**22.52**/**0.6701**/3.24	22.22/0.6323/0.61
	Parrot	19.20/0.5018/**0.03**	21.79/0.6609/0.20	**22.44**/**0.6982**/8.59	21.88/0.6658/0.63
	Books	20.89/0.4826/**0.04**	22.72/0.6791/1.54	**23.36**/**0.7004**/18.86	22.78/0.6562/6.01
gaussian	Circle	27.88/0.6073/**0.03**	31.81/0.8978/0.10	30.19/**0.9240**/2.16	**33.22**/0.9214/0.58
	NCAT	25.45/0.5674/**0.03**	28.91/0.8556/0.18	28.41/0.9070/5.52	**30.93**/**0.9276**/1.09
	Shepp-Logan	19.71/0.5523/**0.03**	21.96/0.5859/0.09	**23.36**/**0.9053**/7.00	22.60/0.7590/0.29
	Cameraman	23.62/0.6125/**0.03**	25.12/0.7547/0.19	**25.42**/**0.7685**/1.98	25.17/0.7484/0.64
	Parrot	23.55/0.6641/**0.04**	25.56/0.7758/0.18	**25.94**/**0.7976**/2.88	25.60/0.7734/0.65
	Books	24.45/0.6602/**0.04**	25.78/0.7797/1.58	**26.77**/**0.8265**/13.75	25.83/0.7749/5.95
disk	Circle	25.91/0.5432/**0.03**	30.64/0.8869/0.12	28.70/0.8879/1.66	**32.28**/**0.9113**/0.64
	NCAT	22.73/0.5030/**0.03**	26.80/0.8179/0.14	26.62/0.8987/11.60	**28.23**/**0.9003**/1.05
	Shepp-Logan	16.87/0.4299/**0.03**	18.56/0.4817/0.12	**19.19**/**0.8044**/11.30	18.64/0.4950/0.22
	Cameraman	21.14/0.4941/**0.03**	22.92/0.6743/0.17	**23.07**/**0.7055**/3.50	23.00/0.6791/0.65
	Parrot	20.22/0.5388/**0.03**	22.37/0.7021/0.18	**22.75**/**0.7227**/10.37	22.48/0.6973/0.63
	Books	22.00/0.5449/**0.04**	23.29/0.7209/1.50	**23.90**/**0.7428**/18.90	23.37/0.7198/6.13
Average values		21.65/0.5146/**0.03**	24.39/0.7179/0.38	24.45/**0.8000**/8.95	**24.98**/0.7419/1.50

Table 3: PSNR, SSIM and Time using different methods for images corrupted by Cauchy noise with $\xi = 0.02$ and $\xi = 0.04$.

ξ	Image	NDE PSNR/SSIM/Time	WNNM PSNR/SSIM/Time	Our PSNR/SSIM/Time
0.02	Circle	32.00/0.7508/0.38	**38.79**/**0.9883**/33.69	38.75/0.9683/**0.17**
	NCAT	30.03/0.6532/0.72	35.26/**0.9892**/79.98	**37.44**/0.9604/**0.57**
	Shepp-Logan	27.05/0.6376/0.19	**29.34**/0.8957/101.34	27.58/**0.9445**/**0.11**
	Cameraman	25.08/0.7442/0.75	**30.14**/**0.8736**/120.96	28.84/0.8615/**0.49**
	Parrot	25.47/0.7612/0.72	**29.82**/**0.9142**/45.91	29.45/0.8749/**0.49**
	Books	22.30/0.7045/13.54	**31.69**/**0.9378**/279.24	30.34/0.9013/**4.98**
0.04	Circle	29.22/0.6547/0.42	**35.77**/**0.9685**/22.54	35.54/0.9355/**0.14**
	NCAT	26.81/0.5378/1.23	31.43/**0.9598**/32.62	**34.11**/0.9338/**0.54**
	Shepp-Logan	23.96/0.5014/0.27	**29.65**/**0.8925**/62.33	27.31/0.8535/**0.15**
	Cameraman	22.99/0.6852/1.28	**29.08**/**0.8635**/125.92	27.13/0.8062/**0.50**
	Parrot	22.93/0.7083/1.25	27.06/**0.8782**/30.07	**27.29**/0.8264/**0.50**
	Books	22.22/0.6945/13.47	**29.17**/**0.8925**/189.69	28.00/0.8520/**4.82**
Average values		25.84/0.6695/2.85	**31.43**/**0.9212**/93.69	30.98/0.8932/**1.12**

be convergent globally. Experimental results demonstrated that our method presented good performances especially for images with more homogeneous regions.

Acknowledgements

The authors would like to thank Profs. Ai, Kim and Shi for sharing the MATLAB codes of image restoration and the reviewers for providing us valuable suggestions to revise this paper. This work was supported by the National Natural Science Foundation of China (NSFC No. 12001144) and Zhejiang Provincial Natural Science Foundation of China (No. LQ20A010007).

References

[1] X. Ai, G. Ni, and T. Zeng, *Nonconvex regularization for blurred images with Cauchy noise*, Inverse Probl. Imag., 16 (2022), pp. 625–646.
[2] H. Attouch, J. Bolte, P. Redont, and A. Soubeyran, *Proximal alternating minimization and projection methods for nonconvex problems: an approach based on the Kurdyka-Łojasiewicz inequality*, Math. Oper. Res., 35 (2008), pp. 438–457.
[3] H. Attouch, J. Bolte, and B. F. Svaiter, *Convergence of descent methods for semi-algebraic and tame problems: proximal algorithms, forward-backward splitting, and regularized Gauss-Seidel methods*, Math. Program., 137 (2013), pp. 91–129.
[4] M. R. Banham and A. K. Katsaggelos, *Digital image restoration*, IEEE Signal Proc. Mag., 14 (1997), pp. 24–41.
[5] W. Bian and X. Chen, *Linearly constrained non-Lipschitz optimization for image restoration*, SIAM J. Imaging Sci., 8 (2015), pp. 2294–2322.
[6] J. Bolte, S. Sabach, and M. Teboulle, *Proximal alternating linearized minimization for nonconvex and nonsmooth problems*, Math. Program., 146 (2014), pp. 459–494.
[7] Y.-C. Chang, S. R. Kadaba, P. C. Doerschuk, and S. B. Gelfand, *Image restoration using recursive Markov random field models driven by Cauchy distributed noise*, IEEE Signal Process. Lett., 8 (2001), pp. 65–66.
[8] X. Chen, L. Niu, and Y. Yuan, *Optimality conditions and a smoothing trust region Newton method for nonlipschitz optimization*, SIAM J. Optim., 23 (2013), pp. 1528–1552.
[9] X. Chen and W. Zhou, *Smoothing nonlinear conjugate gradient method for image restoration using nonsmooth nonconvex minimization*, SIAM J. Imaging Sci., 3 (2010), pp. 765–790.
[10] X. Chen and W. Zhou, *Convergence of the reweighted ℓ_1 minimization algorithm for ℓ_2-ℓ_p minimization*, Comput. Optim. Appl., 59 (2014), pp. 47–61.
[11] L.-J. Deng, H. Guo, and T.-Z. Huang, *A fast image recovery algorithm based on splitting deblurring and denoising*, J. Comput. Appl. Math., 287 (2015), pp. 88–97.
[12] M. Ding, T.-Z. Huang, S. Wang, J.-J. Mei, and X.-L. Zhao, *Total variation with overlapping group sparsity for deblurring images under Cauchy noise*, Appl. Math. Comput., 341 (2019), pp. 128–147.
[13] Y. Gao and C. Wu, *On a general smoothly truncated regularization for variational piecewise constant image restoration: construction and convergent algorithms*, Inverse Probl., 36 (2020), p. 045007.
[14] X. Guo, Y. Xue, and C. Wu, *Effective two-stage image segmentation: a new non-Lipschitz decomposition approach with convergent algorithm*, J. Math. Imag. Vis., 63 (2021), pp. 356–379.
[15] M. Hintermller and T. Wu, *Nonconvex tv^q-models in image restoration: analysis and a trust-region regularization based superlinearly convergent solver*, SIAM J. Imag. Sci., 6 (2013), pp. 1385–1415.

[16] M. JUNG AND M. KANG, *Image restoration under Cauchy noise with sparse representation prior and total generalized variation*, J. Comput. Math., 39 (2021), pp. 81–107.
[17] G. KIM, J. CHO, AND M. KANG, *Cauchy noise removal by weighted nuclear norm minimization*, J. Sci. Comput., 83 (2020), pp. 1–21.
[18] M. J. LAI, Y. XU, AND W. YIN, *Improved iteratively reweighted least squares for unconstrained smoothed ℓ_q minimization*, SIAM J. Numer. Anal., 51 (2013), pp. 927–957.
[19] F. LAUS, F. PIERRE, AND G. STEIDL, *Nonlocal myriad filters for Cauchy noise removal*, J. Math. Imag. Vis., 60 (2018), pp. 1324–1354.
[20] S. LEE AND M. KANG, *Group sparse representation for restoring blurred images with Cauchy noise*, J. Sci. Comput., 83 (2020), pp. 1–27.
[21] J.-J. MEI, Y. DONG, T.-Z. HUANG, AND W. YIN, *Cauchy noise removal by nonconvex ADMM with convergence guarantees*, J. Sci. Comput., 74 (2018), pp. 743–766.
[22] M. K. NG, R. H. CHAN, AND W.-C. TANG, *A fast algorithm for deblurring models with Neumann boundary conditions*, SIAM J. Sci. Comput., 21 (1999), pp. 851–866.
[23] M. NIKOLOVA, *Analysis of the recovery of edges in images and signals by minimizing nonconvex regularized least-squares*, SIAM J. Multiscale Model. Simul., 4 (2005), pp. 960–991.
[24] M. NIKOLOVA, M. K. NG, AND C. P. TAM, *Fast nonconvex nonsmooth minimization methods for image restoration and reconstruction*, IEEE Trans. Image Process., 19 (2010), pp. 3073–3088.
[25] M. NIKOLOVA, M. K. NG, S. ZHANG, AND W. K. CHING, *Efficient reconstruction of piecewise constant images using nonsmooth nonconvex minimization*, SIAM J. Imag. Sci., 1 (2008), pp. 2–25.
[26] P. OCHS, A. DOSOVITSKIY, T. BROX, AND T. POCK, *On iteratively reweighted algorithms for nonsmooth nonconvex optimization in computer vision*, SIAM J. Imag. Sci., 8 (2015), pp. 331–372.
[27] A. PADCHAROEN, P. KUMAM, AND J. MARTÍNEZ-MORENO, *Augmented Lagrangian method for TV-ℓ_1-ℓ_2 based colour image restoration*, J. Comput. Appl. Math., 354 (2019), pp. 507–519.
[28] R. T. ROCKAFELLAR AND R. J.-B. WETS, Variational Analysis, vol. 317, Springer, Berlin, 2009.
[29] L. I. RUDIN, S. OSHER, AND E. FATEMI, *Nonlinear total variation based noise removal algorithms*, Phys. D Nonlinear Phenomena, 60 (1992), pp. 259–268.
[30] F. SCIACCHITANO, Y. DONG, AND T. ZENG, *Variational approach for restoring blurred images with Cauchy noise*, SIAM J. Imag. Sci., 8 (2015), pp. 1894–1922.
[31] K. SHI, G. DONG, AND Z. GUO, *Cauchy noise removal by nonlinear diffusion equations*, Comput. Math. Appl., 80 (2020), pp. 2090–2103.
[32] W. WANG AND Y. CHEN, *An accelerated smoothing gradient method for nonconvex nonsmooth minimization in image processing*, J. Sci. Comput., 90 (2022), pp. 1–28.
[33] W. WANG, C. WU, AND Y. GAO, *A nonconvex truncated regularization and box-constrained model for CT reconstruction*, Inverse Probl. Imag., 14 (2020), pp. 867–890.
[34] W. WANG, C. WU, AND X. C. TAI, *A globally convergent algorithm for a constrained non-Lipschitz image restoration model*, J. Sci. Comput., 83 (2020), pp. 1–29.
[35] Y. WANG, J. YANG, W. YIN, AND Y. ZHANG, *A new alternating minimization algorithm for total variation image reconstruction*, SIAM J. Imag. Sci., 1 (2008), pp. 248–272.
[36] Z. WANG, A. C. BOVIK, H. R. SHEIKH, AND E. P. SIMONCELLI, *Image quality assessment: from error visibility to structural similarity*, IEEE Trans. Image Process., 13 (2004), pp. 600–612.
[37] C. WU AND X. TAI, *Augmented Lagrangian method, dual methods, and split Bregman iteration for ROF, vectorial TV, and high order models*, SIAM J. Imag. Sci., 3 (2010), pp. 300–339.
[38] T. WU, X. GU, Z. LI, Z. LI, J. NIU, AND T. ZENG, *Efficient boosted DC algorithm for nonconvex image restoration with Rician noise*, SIAM J. Imag. Sci., 15 (2022), pp. 424–454.
[39] T. WU, W. LI, S. JIA, Y. DONG, AND T. ZENG, *Deep multi-level wavelet-CNN denoiser prior for*

restoring blurred image with Cauchy noise, IEEE Signal Process. Lett., 27 (2020), pp. 1635–1639.

[40] Z. XU, X. CHANG, F. XU, AND H. ZHANG, *$\ell_{\frac{1}{2}}$ regularization: a thresholding representation theory and a fast solver*, IEEE Trans. Neural Netw. Learn. Syst., 23 (2012), pp. 1013–1027.

[41] H.-Y. YAN AND Y.-M. HUANG, *Cauchy noise removal by a generalized nonlocal low-rank method*, J. Electron. Imag., 31 (2022), p. 033022.

[42] J.-H. YANG, X.-L. ZHAO, J.-J. MEI, S. WANG, T.-H. MA, AND T.-Z. HUANG, *Total variation and high-order total variation adaptive model for restoring blurred images with Cauchy noise*, Comput. Math. Appl., 77 (2019), pp. 1255–1272.

[43] C. ZENG, R. JIA, AND C. WU, *An iterative support shrinking algorithm for non-Lipschitz optimization in image restoration*, J. Math. Imag. Vis., 61 (2019), pp. 122–139.

[44] C. ZENG AND C. WU, *On the edge recovery property of noncovex nonsmooth regularization in image restoration*, SIAM J. Numer. Anal., 56 (2018), pp. 1168–1182.

[45] J. ZHU, J. WEI, H. LV, AND H. BINBIN, *Truncated fractional-order total variation for image denoising under Cauchy noise*, Axioms, 11 (2022), p. 101.